Hot and dense hadronic matter in an effective mean-field approach

A. Lavagno
Dipartimento di Fisica, Politecnico di Torino, I-10129 Torino, Italy and
INFN, Sezione di Torino, I-10126 Torino, Italy
(Received 26 January 2010; revised manuscript received 30 March 2010; published 27 April 2010)

We investigate the equation of state of hadronic matter at finite values of baryon density and temperature reachable in high-energy heavy-ion collisions. The analysis is performed by requiring the Gibbs conditions on the global conservation of baryon number, electric charge fraction, and zero net strangeness. We consider an effective relativistic mean-field model with the inclusion of Δ isobars, hyperons, and the lightest pseudoscalar and vector meson degrees of freedom. In this context, we study the influence of the Δ-isobar degrees of freedom in the hadronic equation of state and, in connection, the behavior of different particle-antiparticle ratios and strangeness production.

DOI: 10.1103/PhysRevC.81.044909 PACS number(s): 21.65.Mn, 25.75.−q

I. INTRODUCTION

The determination of the properties of nuclear matter as functions of density and temperature is a fundamental task in nuclear and subnuclear physics. Heavy-ion collision experiments open the possibility to investigate strongly interacting compressed nuclear matter by exploring in the laboratory the structure of the QCD phase diagram [1–4]. The extraction of information about the equation of state (EOS) at different densities and temperatures by means of intermediate- and high-energy heavy-ion collisions is a very difficult task and can be realized only indirectly by comparing the experimental data with different theoretical models, such as, for example, fluid-dynamical models. The EOS at density below the saturation density of nuclear matter ($\rho_0 \approx 0.16$ fm^{-3}) is relatively well known due to the large amount of experimental nuclear data available. At larger density there are many uncertainties; the strong repulsion at short distances of nuclear force makes, in fact, the compression of nuclear matter quite difficult. However, in relativistic heavy-ion collisions the baryon density can reach values of a few times the saturation nuclear density and/or high temperatures. The future CBM (compressed baryonic matter) experiment of the FAIR (Facility of Antiproton and Ion Research) project at GSI Darmstadt will make it possible to create compressed baryonic matter with a high net baryon density [5–7]. In this direction interesting results have been obtained at low energy at the CERN Super Proton Collider (SPS) and are foreseen at a low-energy scan at BNL Relativistic Heavy Ion Collider (RHIC) [8–12].

Furthermore, the information coming from experiments with heavy ions in intermediate- and high-energy collisions is that the EOS depends on the energy beam but also on the electric charge fraction Z/A of the colliding nuclei, especially at not too high temperature [13,14]. Moreover, the analysis of observations of neutron stars, which are composed of β-stable matter for which $Z/A \leqslant 0.1$, can also provide hints on the structure of extremely asymmetric matter at high density [15,16].

To well understand the structure of the phase diagram and the supposed deconfinement quark-gluon phase transition at large density and finite temperature, it is crucial to know accurately the EOS of the hadronic as well as the quark-gluon phase. Concerning the hadronic phase, hadron resonance gas models have turned out to be very successful in describing particle abundances produced in (ultra)relativistic heavy-ion collisions [17–19]. In this framework, to take phenomenologically into account the interaction between hadrons at finite densities, finite size corrections have been considered in the excluded volume approximation [20–25].

From a more microscopic point of view, the hadronic EOS should reproduce properties of equilibrium nuclear matter such as, for example, saturation density, binding energy, symmetric energy coefficient, and compression modulus. Some other constraints on the behavior of the EOS come from analysis of the experimental flow data of heavy-ion collisions at intermediate energy [26] and, moreover, there are different indirect contraints/indications related to astrophysical bounds on high-density β-equilibrium compact stars [15,27]. In connection with these matters, Walecka-type relativistic mean-field (RMF) models have been widely successfully used for describing the properties of finite nuclei as well as dense and finite temperature nuclear matter [28–32]. It is relevant to point out that such RMF models usually do not respect chiral symmetry. Furthermore, the repulsive vector field is proportional to the net baryon density; therefore, standard RMF models do not appear, in principle, fully appropriate for very low-density and high-temperature regimes. In this context, let us observe that a phenomenological RMF model has been recently proposed to calculate the EOS of hadronic matter in a broad density-temperature region by considering masses and coupling constants depending on the σ-meson field [33]. In that approach, motivated by the Brown-Rho scaling hypothesis, a nonchiral symmetric model simulates a chiral symmetric restoration with a temperature increase. However, sophisticated relativistic chiral SU(3) models have also been developed to take into account particle ratios at RHIC and baryon resonances impact on the chiral phase transition [34,35].

In a regime of finite values of density and temperature, a state of high-density resonance matter may be formed and the $\Delta(1232)$-isobar degrees of freedom are expected to play a central role [36]. Transport model calculations and experimental results indicate that an excited state of baryonic matter is dominated by the Δ resonance at the energies

from the BNL Alternating Gradien Synchrotron (AGS) to RHIC [37–42]. Moreover, in the framework of the nonlinear Walecka model, it has been predicted that a phase transition from nucleonic matter to Δ-excited nuclear matter can take place and the occurrence of this transition sensibly depends on the Δ-meson coupling constants [43,44]. Referring to QCD finite-density sum rule results, which predict that there is a larger net attraction for a Δ isobar than for a nucleon in the nuclear medium [45], the range of values for the Δ-meson coupling constants has been confined within a triangle relation [46]. Whether stable Δ-excited nuclear matter exists or not is still a controversial issue because little is actually known about the Δ coupling constants with the scalar and vector mesons. In any case, it has been pointed out that the existence of degrees of freedom related to Δ isobars can be very relevant in relativistic heavy-ion collisions and in the core of neutron stars [44,47,48]. Although several articles have investigated the influence of Δ isobars on the nuclear EOS, we believe that, especially in presence of asymmetric and strange hadronic matter, a systematic investigation at finite densities and temperatures has been lacking.

In this article, we study the hadronic EOS by means of an effective RMF model with the inclusion of the full octet of baryons, the Δ-isobar degrees of freedom, and the lightest pseudoscalar and vector mesons. These last particles are considered in the so-called one-body contribution, taking into account their effective chemical potentials depending on the self-consistent interaction between baryons. The main goal is to investigate how the constraints on the global conservation of the baryon number, electric charge fraction, and strangeness neutrality, in the presence of Δ-isobar degrees of freedom, hyperons, and strange mesons, influence the behavior of the EOS in a regime of finite values of baryon density and temperature. Moreover, we show the relevance of Δ isobars for different coupling constants and how their presence influences several particle ratios and strangeness production for three different parameters sets, compatible with experimental constraints.

This article is organized as follows. In Sec. II, we present the model with a detailed discussion on the hyperon-meson couplings and on the chemical equilibrium conditions. To better clarify the role of Δ isobars and strange particles in symmetric and asymmetric nuclear matter, our results are presented in Sec. III, which is divided into three subsections: in A, we study the equation of state of nucleons and Δ isobars in symmetric nuclear matter at zero and finite temperature; in B, the investigation is extended by including hyperons, non-strange mesons, and strange mesons in asymmetric nuclear matter and by requiring the zero net strangeness condition; and in C, strangeness production and different particle-antiparticle ratios are considered. Finally, the main conclusions are summarized in Sec. IV.

II. HADRONIC EQUATION OF STATE

The basic idea of the RMF model, first introduced by Walecka [49] and Boguta and Bodmer [50] in the mid-1970s, is the interaction between baryons through the exchange of mesons. In the original version we have an isoscalar-scalar σ meson field which produces the medium range attraction and the exchange of isoscalar-vector ω mesons responsible for the short range repulsion. The saturation density and binding energy per nucleon of nuclear matter can be fitted exactly in the simplest version of this model but other properties of nuclear matter, for example, incompressibility, cannot be well reproduced. To overcome these difficulties, the model has been modified introducing in the Lagrangian two terms of self-interaction for the σ mesons that are crucial to reproduce the empirical incompressibility of nuclear matter and the effective mass of nucleons M_N^*. Moreover, the introduction of an isovector-vector ρ meson allows one to reproduce the correct value of the empirical symmetry energy [51], and an isovector-scalar field, a virtual $a_0(980)$ δ meson, has been been studied for asymmetric nuclear matter and for heavy-ion collisions [13,52].

The total Lagrangian density $\mathcal{L}$ can be written as

$$\mathcal{L} = \mathcal{L}_{\rm om} + \mathcal{L}_{\Delta} + \mathcal{L}_{\rm qfm}, \tag{1}$$

where $\mathcal{L}_{\rm om}$ stands for the full octet of the lightest baryons (p, n, Λ, Σ^+, Σ^0, Σ^-, Ξ^0, Ξ^-) interacting with σ-, ω-, ρ-, δ-meson fields; $\mathcal{L}_{\Delta}$ corresponds to the degrees of freedom for the Δ isobars (Δ^{++}, Δ^+, Δ^0, Δ^-), and $\mathcal{L}_{\rm qfm}$ is related to a (quasi)free gas of the lightest pseudoscalar and vector mesons with an effective chemical potential (details are given later in this article). In regime of density and temperature in which we are mostly interested, we expect that the inclusion of the other decuplet baryons will produce only a small change in the overall results.

The RMF model for the self-interacting full octet of baryons ($J^P = 1/2^+$) was originally studied by Glendenning [53] with the following standard Lagrangian,

$$\begin{aligned}\mathcal{L}_{\rm om} = \sum_k \overline{\psi}_k [& i\gamma_\mu \partial^\mu - (M_k - g_{\sigma k}\sigma - g_{\delta k}\vec{t}\cdot\vec{\delta}) - g_{\omega k}\gamma_\mu \omega^\mu \\ & - g_{\rho k}\gamma_\mu \vec{t}\cdot\vec{\rho}^{\,\mu}]\psi_k + \frac{1}{2}\left(\partial_\mu\sigma\partial^\mu\sigma - m_\sigma^2\sigma^2\right) - U(\sigma) \\ & + \frac{1}{2}m_\omega^2\omega_\mu\omega^\mu + \frac{1}{4}c\left(g_{\omega N}^2\omega_\mu\omega^\mu\right)^2 + \frac{1}{2}m_\rho^2\vec{\rho}_\mu\cdot\vec{\rho}^{\,\mu} \\ & + \frac{1}{2}\left(\partial_\mu\vec{\delta}\partial^\mu\vec{\delta} - m_\delta^2\vec{\delta}^2\right) - \frac{1}{4}F_{\mu\nu}F^{\mu\nu} - \frac{1}{4}\vec{G}_{\mu\nu}\vec{G}^{\mu\nu},\end{aligned} \tag{2}$$

where the sum runs over the full octet of baryons, M_k is the vacuum baryon mass of index k, the quantity $\vec{t}$ denotes the isospin operator that acts on the baryon, and the field strength tensors for the vector mesons are given by the usual expressions $F_{\mu\nu} \equiv \partial_\mu\omega_\nu - \partial_\nu\omega_\mu$ and $\vec{G}_{\mu\nu} \equiv \partial_\mu\vec{\rho}_\nu - \partial_\nu\vec{\rho}_\mu$. The $U(\sigma)$ is a nonlinear self-interaction potential of the σ meson,

$$U(\sigma) = \tfrac{1}{3}a(g_{\sigma N}\sigma)^3 + \tfrac{1}{4}b(g_{\sigma N}\sigma^4), \tag{3}$$

introduced by Boguta and Bodmer [50] to achieve a reasonable compressibility for equilibrium normal nuclear matter. We have also taken into account the additional self-interaction ω-meson field, $c(g_{\omega N}^2\omega_\mu\omega^\mu)^2/4$, suggested by Bodmer [54] to get a good agreement with Dirac-Brückner calculations at high density and to achieve a more satisfactory description of the properties of finite nuclei in the mean-field approximation.

By taking into account only the on-shell Δ's, the Lagrangian density concerning the Δ isobars can be expressed as [44]

$$\mathcal{L}_\Delta = \overline{\psi}_{\Delta\nu}[i\gamma_\mu\partial^\mu - (M_\Delta - g_{\sigma\Delta}\sigma) - g_{\omega\Delta}\gamma_\mu\omega^\mu]\psi^\nu_\Delta, \quad (4)$$

where ψ^ν_Δ is the Rarita-Schwinger spinor for the Δ baryon. Because of the uncertainty on the Δ-meson coupling constants, we limit ourselves to consider only the coupling with the σ- and ω-meson fields, more of which are explored in the literature [43–46].

In the RMF approach, baryons are considered as Dirac quasiparticles moving in classical mesons fields and the field operators are replaced by their expectation values. In this context, it is relevant to remember that the RMF model does not respect chiral symmetry and the contribution coming from the Dirac sea and the quantum fluctuation of the meson fields are neglected. As a consequence, the field equations in the RMF approximation have the following form

$$(i\gamma_\mu\partial^\mu - M^*_k - g_{\omega k}\gamma^0\omega - g_{\rho k}\gamma^0 t_{3k}\rho)\psi_k = 0, \quad (5)$$

$$(i\gamma_\mu\partial^\mu - M^*_\Delta - g_{\omega\Delta}\gamma^0\omega)\psi_\Delta = 0, \quad (6)$$

$$m^2_\sigma\sigma + ag^3_{\sigma N}\sigma^2 + bg^4_{\sigma N}\sigma^3 = \sum_i g_{\sigma i}\rho^S_i, \quad (7)$$

$$m^2_\omega\omega + cg^4_{\omega N}\omega^3 = \sum_i g_{\omega i}\rho^B_i, \quad (8)$$

$$m^2_\rho\rho = \sum_i g_{\rho i}t_{3i}\rho^B_i, \quad (9)$$

$$m^2_\delta\delta = \sum_i g_{\delta i}t_{3i}\rho^S_i, \quad (10)$$

where $\sigma = \langle\sigma\rangle, \omega = \langle\omega^0\rangle, \rho = \langle\rho^0_3\rangle$, and $\delta = \langle\delta_3\rangle$ are the non-vanishing expectation values of mesons fields. The effective mass of kth baryon octet, in Eq. (5), is given by

$$M^*_k = M_k - g_{\sigma k}\sigma - g_{\delta k}t_{3k}\delta, \quad (11)$$

and the effective mass of Δ-isobar, in Eq. (6), is given by

$$M^*_\Delta = M_\Delta - g_{\sigma\Delta}\sigma. \quad (12)$$

In the meson-field equations, Eqs. (7)–(10), the sums run over all considered baryons (octet and Δ's) and ρ^B_i and ρ^S_i are the baryon density and the baryon scalar density of the particle of index i, respectively. They are given by

$$\rho^B_i = \gamma_i\int\frac{\mathrm{d}^3k}{(2\pi)^3}[f_i(k) - \overline{f}_i(k)], \quad (13)$$

$$\rho^S_i = \gamma_i\int\frac{\mathrm{d}^3k}{(2\pi)^3}\frac{M^*_i}{E^*_i}[f_i(k) + \overline{f}_i(k)], \quad (14)$$

where $\gamma_i = 2J_i + 1$ is the degeneracy spin factor of the ith baryon ($\gamma_{\text{octet}} = 2$ for the baryon octet and $\gamma_\Delta = 4$) and $f_i(k)$ and $\overline{f}_i(k)$ are the fermion particle and antiparticle distributions:

$$f_i(k) = \frac{1}{\exp\{(E^*_i(k) - \mu^*_i)/T\} + 1}, \quad (15)$$

$$\overline{f}_i(k) = \frac{1}{\exp\{(E^*_i(k) + \mu^*_i)/T\} + 1}. \quad (16)$$

The baryon effective energy is defined as $E^*_i(k) = \sqrt{k^2 + {M_i}^{*2}}$. The chemical potentials μ_i are given in terms of the effective chemical potentials μ^*_i by means of the following relation,

$$\mu_i = \mu^*_i + g_{\omega i}\omega + g_{\rho i}t_{3i}\rho, \quad (17)$$

where t_{3i} is the third component of the isospin of the ith baryon.

Because we are going to describe the nuclear EOS at finite density and temperature with respect to strong interaction, we have to require the conservation of three "charges": baryon number (B), electric charge (C), and strangeness number (S). Each conserved charge has a conjugated chemical potential and the systems is described by three independent chemical potentials: μ_B, μ_C, and μ_S. Therefore, the chemical potential of particle of index i can be written as

$$\mu_i = b_i\mu_B + c_i\mu_C + s_i\mu_S, \quad (18)$$

where b_i, c_i, and s_i are, respectively, the baryon, the electric charge, and the strangeness quantum numbers of ith hadronic species.

The thermodynamical quantities can be obtained from the grand potential Ω_B in the standard way. More explicitly, the baryon pressure $P_B = -\Omega_B/V$ and the energy density ϵ_B can be written as

$$\begin{aligned}P_B = {}& \frac{1}{3}\sum_i\gamma_i\int\frac{\mathrm{d}^3k}{(2\pi)^3}\frac{k^2}{E^*_i(k)}[f_i(k) + \overline{f}_i(k)] \\ & - \frac{1}{2}m^2_\sigma\sigma^2 - U(\sigma) + \frac{1}{2}m^2_\omega\omega^2 + \frac{1}{4}c(g_{\omega N}\omega)^4 \\ & + \frac{1}{2}m^2_\rho\rho^2 - \frac{1}{2}m^2_\delta\delta^2, \end{aligned} \quad (19)$$

$$\begin{aligned}\epsilon_B = {}& \sum_i\gamma_i\int\frac{\mathrm{d}^3k}{(2\pi)^3}\,E^*_i(k)[f_i(k) + \overline{f}_i(k)] \\ & + \frac{1}{2}m^2_\sigma\sigma^2 + U(\sigma) + \frac{1}{2}m^2_\omega\omega^2 + \frac{3}{4}c(g_{\omega N}\omega)^4 \\ & + \frac{1}{2}m^2_\rho\rho^2 + \frac{1}{2}m^2_\delta\delta^2. \end{aligned} \quad (20)$$

The numerical evaluation of theses thermodynamical quantities can be performed if the meson-nucleon, meson-Δ, and meson-hyperon coupling constants are known. Concerning the meson-nucleon coupling constants ($g_{\sigma N}$, $g_{\omega N}$, $g_{\rho N}$, $g_{\delta N}$), they are determined to reproduce properties of equilibrium nuclear matter such as the saturation densities, the binding energy, the symmetric energy coefficient, the compression modulus, and the effective Dirac mass at saturation. Because of a valuable range of uncertainty in the empirical values that must be fitted, especially for the compression modulus and for the effective Dirac mass, in the literature there are different sets of coupling constants. In Table I, we report the parameters sets used in this work. The set marked GM3 is from Glendenning and Moszkowski [55], that labeled NL$\rho\delta$ is from Refs. [52,56], and that labeled TM1 is from Ref. [57]. As evident in the

TABLE I. Nuclear matter properties and nucleon coupling constants of the parameters sets used in the calculation. The energy per particle is $E/A = 16.3$ MeV, calculated at the saturation density ρ_0 with a compression modulus K and effective mass M_N^* (the nucleon mass M_N is fixed to 939 MeV for GM3 and NL$\rho\delta$, and $M_N = 938$ MeV in the TM1 parameters set). The symmetry energy is denoted by $a_{\rm sym}$. In the parameter set NL$\rho\delta$ the additional coupling to the δ meson is fixed to $g_{\delta N}/m_\delta = 3.162$ fm.

	ρ_0 (fm^{-3})	K (MeV)	M_N^*/M_N	$a_{\rm sym}$ (MeV)	$\frac{g_{\sigma N}}{m_\sigma}$ (fm)	$\frac{g_{\omega N}}{m_\omega}$ (fm)	$\frac{g_{\rho N}}{m_\rho}$ (fm)	a (fm^{-1})	b	c
GM3	0.153	240	0.78	32.5	3.151	2.195	2.189	0.04121	−0.00242	–
NL$\rho\delta$	0.160	240	0.75	30.5	3.214	2.328	3.550	0.0330	−0.0048	–
TM1	0.145	281	0.63	36.9	3.871	3.178	2.374	0.00717	0.00006	0.00282

next section, we have limited our investigation to these three parameters sets that are compatible with intermediate heavy-ion collision constraints and extensively used in various high-density astrophysical applications. Please note that the first two parameters sets have the same saturated compressibility K and an almost equal value of the nucleon effective mass M_N^*, significantly larger than the TM1 one. Therefore, the GM3 and NL$\rho\delta$ models will fail to reproduce the correct spin-orbit splittings in finite nuclei [58]. However, the TM1 parameter set has a larger value of K but a sensibly lower value of M_N^*. As will be seen, these different saturation properties of nuclear matter are strongly correlated with the formation of Δ-isobar matter at finite density and temperature.

The implementation of hyperon degrees of freedom comes from determination of the corresponding meson-hyperon coupling constants that have been fitted to hypernuclear properties. Following Refs. [59–63], the SU(6) simple quark model can be used to obtain the relations

$$\begin{aligned} \tfrac{1}{3}g_{\omega N} &= \tfrac{1}{2}g_{\omega\Lambda} = \tfrac{1}{2}g_{\omega\Sigma} = g_{\omega\Xi}, \\ g_{\rho N} &= \tfrac{1}{2}g_{\rho\Sigma} = g_{\rho\Xi}, \quad g_{\rho\Lambda} = 0, \\ g_{\delta N} &= \tfrac{1}{2}g_{\delta\Sigma} = g_{\delta\Xi}, \quad g_{\delta\Lambda} = 0. \end{aligned} \tag{21}$$

In addition, we can fix the scalar σ-meson–hyperon ($g_{\sigma Y}$) coupling constants to the potential depth of the corresponding hyperon in normal dense matter taking into account the following recent results [63–66]:

$$U_\Lambda^N = -28\,\mathrm{MeV}, \quad U_\Sigma^N = +30\,\mathrm{MeV}, \quad U_\Xi^N = -18\ \mathrm{MeV}. \tag{22}$$

In Table II, the obtained ratios $x_{\sigma Y} = g_{\sigma Y}/g_{\sigma N}$ are reported, and the vacuum hyperon masses are listed in Table III. In this context, note that the two additional meson fields $f_0(975)$ and $\phi(1020)$, usually introduced to simulate the hyperon-hyperon attraction observed in Λ-Λ hypernuclei [62,63], do not play a significant role in the considered range of density and temperature and, therefore, their contributions are neglected.

TABLE II. Ratios of the scalar σ-meson coupling constants for hyperons: $x_{\sigma Y} = g_{\sigma Y}/g_{\sigma N}$.

	$x_{\sigma\Lambda}$	$x_{\sigma\Sigma}$	$x_{\sigma\Xi}$
GM3	0.606	0.328	0.322
NL$\rho\delta$	0.606	0.361	0.320
TM1	0.616	0.447	0.319

As discussed in the Introduction, the aim of this work is to describe the EOS at finite values of density and temperature. Especially at low baryon density and high temperature, the contribution of the lightest pseudoscalar and vector mesons to the total thermodynamical potential (and, consequently, to the other thermodynamical quantities) becomes very important. However, the contribution of the π mesons (and other pseudoscalar and pseudovector fields) vanishes at the mean-field level. From a phenomenological point of view, we can take into account the meson particle degrees of freedom by adding their one-body contribution to the thermodynamical potential, that is, the contribution of an ideal Bose gas with an effective chemical potential μ_j^*, depending self-consistently from the meson fields. Following this scheme, it is possible to evaluate the pressure P_M, the energy density ϵ_M, and the particle density ρ_j^M of mesons as

$$P_M = \frac{1}{3}\sum_j \gamma_j \int \frac{\mathrm{d}^3k}{(2\pi)^3}\,\frac{k^2}{E_j(k)}\,g_j(k), \tag{23}$$

$$\epsilon_M = \sum_j \gamma_j \int \frac{\mathrm{d}^3k}{(2\pi)^3}\,E_j(k)\,g_j(k), \tag{24}$$

$$\rho_j^M = \gamma_j \int \frac{\mathrm{d}^3k}{(2\pi)^3}\,g_j(k), \tag{25}$$

where $\gamma_j = 2J_j + 1$ is the degeneracy spin factor of the jth meson ($\gamma = 1$ for pseudoscalar mesons and $\gamma = 3$ for vector mesons), the sum runs over the lightest pseudoscalar mesons (π, K, $\overline{K}$, η, η') and the lightest vector mesons (ρ, ω, K^*, $\overline{K}^*$, ϕ), considering the contribution of particle and antiparticle separately. In Eqs. (23)–(25) the function $g_j(k)$ is the boson particle distribution (the corresponding antiparticle distribution $\overline{g}_j(k)$ will be obtained with the substitution $\mu_j^* \to -\mu_j^*$) given by

$$g_j(k) = \frac{1}{\exp\{(E_j(k) - \mu_j^*)/T\} - 1}, \tag{26}$$

where $E_j(k) = \sqrt{k^2 + m_j^2}$ and m_j is the jth meson mass (see Table III). Moreover, the boson integrals are subjected to the constraint $|\mu_j^*| \leqslant m_j$, otherwise Bose condensation becomes possible (as seen in the next section, this condition is never achieved in the range of density and temperature investigated in this article). The values of the effective meson

TABLE III. Vacuum masses (given in MeV) of the considered hadronic particles.

M_N	M_Λ	M_Σ	M_Δ	M_Ξ	M_π	M_K	M_η	$M_{\eta'}$	M_{K^*}	M_ρ	M_ω	M_ϕ
939	1116	1189	1232	1315	140	494	547	958	892	771	782	1020

chemical potentials μ_j^* are obtained from the "bare" ones μ_j, given in Eq. (18), and subsequently expressed in terms of the corresponding effective baryon chemical potentials, respecting the strong interaction.[1] For example, we have from Eq. (18) that $\mu_{\pi^+} = \mu_{\rho^+} = \mu_C \equiv \mu_p - \mu_n$ and the corresponding effective chemical potential can be written as

$$\begin{aligned}\mu^*_{\pi^+(\rho^+)} &\equiv \mu_p^* - \mu_n^* \\ &= \mu_p - \mu_n - g_{\rho N}\rho, \end{aligned} \tag{27}$$

where the last equivalence follows from Eq. (17).

Analogously, by setting $x_{\omega\Lambda} = g_{\omega\Lambda}/g_{\omega N}$, we have

$$\begin{aligned}\mu^*_{K^+(K^{*+})} &\equiv \mu_p^* - \mu^*_{\Lambda(\Sigma^0)} \\ &= \mu_p - \mu_\Lambda - (1 - x_{\omega\Lambda})g_{\omega N}\omega - \tfrac{1}{2}g_{\rho N}\rho, \end{aligned} \tag{28}$$

$$\begin{aligned}\mu^*_{K^0(K^{*0})} &\equiv \mu_n^* - \mu^*_{\Lambda(\Sigma^0)} \\ &= \mu_n - \mu_\Lambda - (1 - x_{\omega\Lambda})g_{\omega N}\omega + \tfrac{1}{2}g_{\rho N}\rho, \end{aligned} \tag{29}$$

while the others' strangeless neutral mesons have a vanishing chemical potential. Thus, the effective meson chemical potentials are coupled with the meson fields related to the interaction between baryons. As seen in the next section, this assumption represents a crucial feature in the EOS at finite density and temperature and can be seen somehow in analogy with the hadron resonance gas within the excluded-volume approximation. There the hadronic system is still regarded as an ideal gas but in the volume reduced by the volume occupied by constituents (usually assumed as a phenomenological model parameter), here we have a (quasifree) meson gas but with an effective chemical potential that contains the self-consistent interaction of the meson fields.

Finally, the total pressure and energy density will be

$$P = P_B + P_M, \tag{30}$$

$$\epsilon = \epsilon_B + \epsilon_M. \tag{31}$$

At a given temperature T, all the aforementioned equations must be evaluated self-consistently by requiring the conservation of the baryon, electric charge fraction, and strangeness numbers [68]. Therefore, at a given baryon density ρ_B, a given Z/A net electric charge fraction ($\rho_C = Z/A\rho_B$) and a zero net strangeness of the system ($\rho_S = 0$), the chemical potentials μ_B, μ_C, and μ_S are univocally determined by the following equations

$$\rho_B = \sum_i b_i \rho_i(T, \mu_B, \mu_C, \mu_S), \tag{32}$$

$$\rho_C = \sum_i c_i \rho_i(T, \mu_B, \mu_C, \mu_S), \tag{33}$$

$$\rho_S = \sum_i s_i \rho_i(T, \mu_B, \mu_C, \mu_S), \tag{34}$$

where the sums run over all considered particles.

III. RESULTS AND DISCUSSION

A. Equation of state of pnΔ symmetric nuclear matter

Let us start our numerical investigation by considering the symmetric hadronic EOS using the model discussed here. To better focalize the role of Δ-isobar degrees of freedom, this first subsection is limited to the consideration of only protons, neutrons, and Δ particles.

In Fig. 1, the pressure as a function of the baryon density (in units of the nuclear saturation density ρ_0) in the limit of zero temperature is reported. Among the several parameter sets, we choose the three sets, GM3, NL$\rho\delta$, and TM1 (see Table I for details), that meet in a satisfactory way the region, reported as the shaded area, of pressures consistent with the experimental flow data of heavy-ion collisions at intermediate energy, analyzed by using the Boltzmann equation model [26]. Furthermore, these parameters sets are largely used to describe the hadronic EOS on high-density β-equilibrium compact stars [13,27,32].

At the scope of giving a roughly indication of the presence of the Δ-isobar degrees of freedom from the point of view of the stiffness of the EOS, in Fig. 1, we show the behavior of the pressure corresponding only to nucleons (monotonic curves) and nucleons and Δ (nonmonotonic curves) with the scalar $r_s = g_{\sigma\Delta}/g_{\sigma N}$ and vector $r_v = g_{\omega\Delta}/g_{\omega N}$ meson-Δ coupling ratios. Let us note in this context that, when a metastable condition for Δ isobars is not realized (see subsequent discussion), decays rates are not taken into account. Moreover, a further softening of the EOS can occur considering

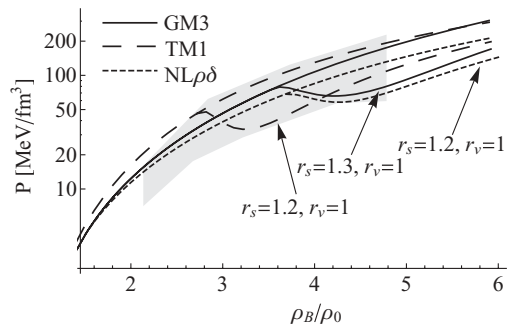

FIG. 1. Pressure as a function of the baryon density (in units of the nuclear saturation density ρ_0) for the symmetric nuclear matter at zero temperature for three different EOSs and Δ coupling ratios (absence of Δ contribution in the monotonic curves). The shaded region corresponds to the limits obtained from the analysis of Ref. [26].

[1] An analog assumption, limited to the pions' contribution, has been, for example, adopted in Ref. [67].

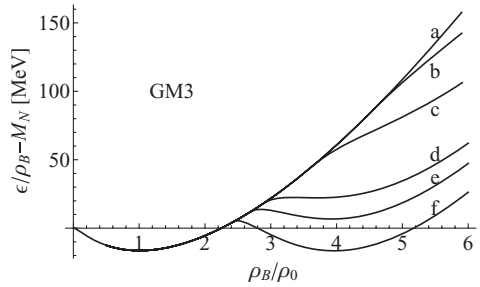

FIG. 2. The energy per baryon versus baryon density at zero temperature and GM3 parameter set with (a) without Δ; (b) non-interacting Δ ($r_s = r_v = 0$); (c) $r_s = 1.3$, $r_v = 1$, (d) $r_s = 1.41$, $r_v = 1$), (e) $r_s = 1.45$, $r_v = 1$, (f) $r_s = 1.5$, $r_v = 1$.

the degrees of freedom of the other hadronic particles. At zero temperature and symmetric nuclear matter these effects occur at very high density and, as anticipated, are considered separately in the next subsections.

To better understand the dependence of the EOS on the meson-Δ coupling constants for the different parameters sets, we start by reporting in Fig. 2 the energy per baryon versus baryon density at zero temperature and GM3 parameter set. The curves (labeled with a, b, c, d, e, f) represent different values of the scalar r_s and vector r_v meson-Δ coupling ratios. In setting these coupling constants we have required, as in Ref. [46], that (i) the second minimum of the energy per baryon lies above the saturation energy of normal nuclear matter, that is, in the mixed Δ-nucleon phase only a metastable state can occur; (ii) there are no Δ isobars present at the saturation density; and (iii) the scalar field is more (equal) attractive and the vector potential is less (equal) repulsive for Δ's than for nucleons, in accordance with QCD finite-density calculations [45]. Of course, the choice of couplings that satisfies the these conditions is not unique but exists as a finite range of possible values (represented as a triangle region in the plane r_s-r_v) that depends on the particular EOS under consideration [46]. Without loss of generality, we can limit our investigation to move only in a side of such a triangle region by fixing $r_v = 1$ and varying r_s from unity to a maximum value compatible with the aforementioned conditions. Similar conclusions are obtained with any other compatible choice of the two coupling ratios.

In Fig. 3, we compare the energy per baryon for different parameters sets but at a fixed value of the scalar and vector Δ coupling constants. At variance of the parameters sets there

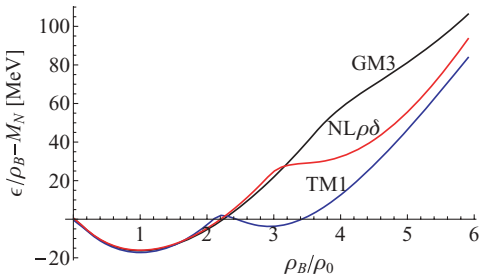

FIG. 3. (Color online) The same as Fig. 2 but for different parameter sets and fixed $r_s = 1.3$ and $r_v = 1$.

TABLE IV. Values of the $r_s^{\rm II}$ corresponding to the appearance of the second minimum on the energy per baryon and the maximum values $r_s^{\rm max}$ obtained by requiring that in the mixed Δ-nucleon phase only a metastable state can occur.

	GM3	NL$\rho\delta$	TM1
$r_s^{\rm II}$	1.41	1.32	1.27
$r_s^{\rm max}$	1.50	1.41	1.33

is a very different behavior; however, comparable features for the three considered parameters sets are obtained by means of a rescaling of the Δ couplings. To better clarify this aspect, Table IV shows, for the three parameters sets and fixing $r_v = 1$, the values of $r_s^{\rm II}$ corresponding to the appearance of the second minimum on the energy per baryon and the values of $r_s^{\rm max}$ corresponding to the maximum values of r_s compatible with the constraint that the second minimum of the energy per baryon lies above the saturation energy of normal nuclear matter.

To get a deeper insight into the dependence of the Δ isobars from the coupling constants and from the temperature, in Fig. 4 the behavior of the effective mass M_Δ^* for different temperatures and Δ coupling constants ($r_s = r_v = 1$ for upper curves and $r_s = 1.32$ and $r_v = 1$ for lower curves) in the NL$\rho\delta$ parameter set is shown. Note that the coupling ratio of the lower curves corresponds to the appearance of the second minimum of the energy per baryon at zero temperature (metastable state). As we can see, the different behavior of the effective Δ mass from the coupling constants is strongly linked to the different behavior of the energy per baryon versus baryon density and temperature.

Figure 5 shows the energy per baryon as a function of the baryon density at $T = 40$–100 MeV for two different Δ scalar coupling ratios r_s and for the TM1 parameter set. As stated before, at zero temperature and fixed $r_v = 1$, there is no second minimum if $r_s = 1$ while it takes place if $r_s = 1.3$ (see Fig. 3 and Table IV). As the temperature increases, the behavior is remarkably different in the case of $r_s = 1.3$ where the first minimum disappears and only the second minimum remains. In Figs. 4 and 5, the results are reported only for one parameter set; however, similar behaviors are obtained with

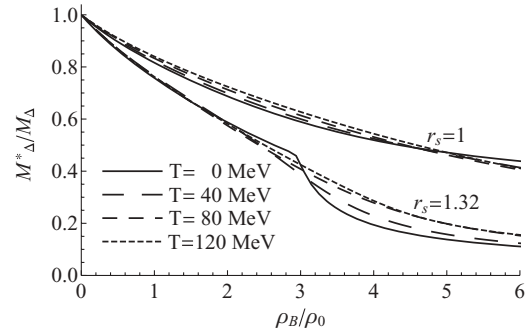

FIG. 4. The Δ effective mass ratios versus the baryon density with $r_s = r_v = 1$ (upper curves) and with $r_s = 1.32$ and $r_v = 1$ (lower curves) for different temperatures. The parameter set used in the calculation is NL$\rho\delta$.

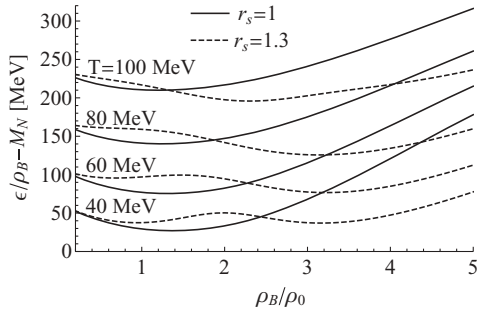

FIG. 5. The energy per baryon versus baryon density for symmetric nuclear matter at different values of temperature and TM1 parameter set. The solid lines correspond to the Δ coupling ratios $r_s = r_v = 1$ and the dashes lines correspond to $r_s = 1.3$ and $r_v = 1$.

the other sets, if we use comparable meson-Δ coupling ratios. To better clarify this aspect, Fig. 6 shows the variation of the baryon density, with respect to temperature, corresponding to the position of the second minimum of the energy per baryon for the three different parameter sets. In the comparison, r_s is fixed to the average value r_m between the values $r_s^{\rm II}$ and $r_s^{\rm max}$ listed in Table IV for each parameters sets ($r_s = 1.46$ for GM3, $r_s = 1.37$ for NL$\rho\delta$, $r_s = 1.30$ for TM1). For all three sets, the position of the second minimum appears approximately at a constant value of baryon density $\rho_B \approx 3$–$4\ \rho_0$ until $T \approx 80$–100 MeV. At higher temperatures, as observed in Fig. 5, the first minimum disappears and the second minimum moves rapidly at lower baryon densities. At fixed temperature, the different positions of the second minimum are a direct consequence of the different saturated nucleon effective mass M_N^* in the considered parameter sets. In agreement with the results of Ref. [44], we see, in fact, that a smaller value of M_N^* favors the appearance of a second minimum of the energy per baryon at a lower baryon density. Therefore, as a result the position of the second minimum is at a sensibly lower baryon density for the TM1 set with respect to the NL$\rho\delta$ and GM3 ones.

Figure 7 shows the nucleon (solid lines) and the Δ-isobar (dashed lines) density, normalized to the baryon density, versus the baryon density for different values of temperature (in MeV). We observe that, although the Δ-isobar density seems to be negligible at low temperatures up to very high densities, it becomes relevant by increasing the temperature even for $r_s = r_v = 1$ (upper panel). Moreover, in the case of $r_s = 1.32$ and $r_v = 1$ (lower panel), the Δ-particle density becomes comparable to the nucleon density in the range of $T \approx 80$–120 MeV and $\rho_B \approx 1$–$2.5\ \rho_0$; values that can be reached in high-energy heavy-ion collisions. This behavior has been obtained for the NL$\rho\delta$ parameter set but is common for all three considered sets even if, at fixed temperature and baryon density, different values of particle densities are obtained for different EOSs. To better focus this matter of fact, in Fig. 8, the variation of the baryon density, as a function of temperature, for which Δ-isobar density is equal to nucleon density ($\rho_\Delta = \rho_N = \rho_B/2$), for the three different parameter sets is reported.

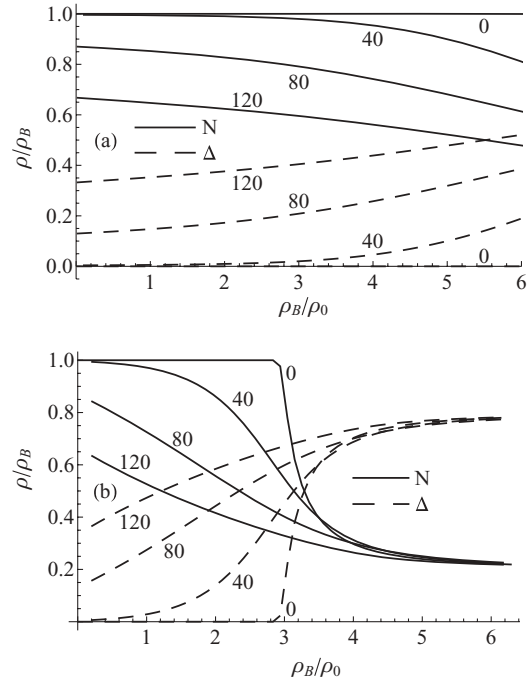

FIG. 7. The relative nucleon (solid lines) and Δ (dashed lines) density versus the baryon density with $r_s = r_v = 1$ (upper panel) and with $r_s = 1.32$ and $r_v = 1$ (lower panel) for different values of temperature (in MeV). The parameter set used in the calculation is NL$\rho\delta$.

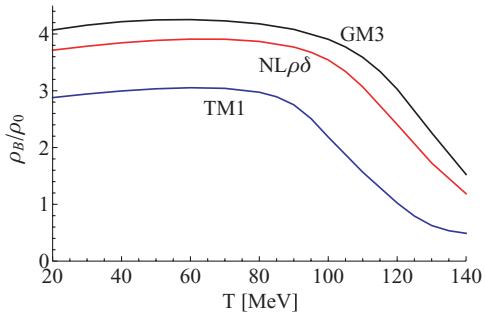

FIG. 6. (Color online) Variation of the baryon density, with respect to temperature, corresponding to the position of the second minimum of the energy per baryon for different parameter sets (see text for details).

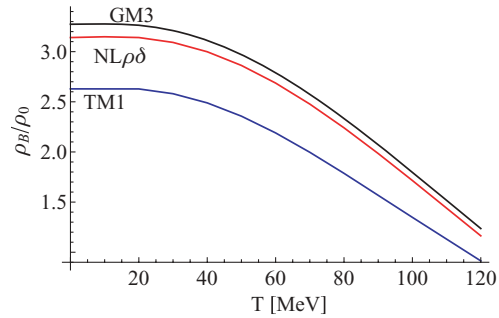

FIG. 8. (Color online) Variation of baryon density, as a function of temperature, for which Δ-isobar density is equal to nucleon density, for different parameter sets. The scalar coupling ratios for each EOS are the values $r_s = r_s^{\rm II}$ reported in Table IV.

Also in this case, in the comparison, comparable values of r_s for different EOSs are used. As in Fig. 7, for the NL$\rho\delta$ parameter set we fix $r_s = 1.32$, corresponding to the value $r_s^{\rm II}$ of Table IV. Analogously, we use $r_s = 1.41$ for GM3 and $r_s = 1.27$ for TM1. As already observed in Fig. 6, for the TM1 parameter set, which has a lower value of M_N^*, the formation of Δ isobars occurs at lower baryon densities with respect to NL$\rho\delta$ and GM3 (with larger values of M_N^*). Small variations between NL$\rho\delta$ and GM3 correspond mainly to the almost equal saturated nucleon effective mass (slightly greater for the GM3 parameter set).

Finally, in agreement with previous investigations [43,44], note that, in Fig. 7, the ρ_Δ/ρ_B and ρ_N/ρ_B ratios become constant at sufficiently high baryon density, regardless of the temperature. By increasing the r_s ratio (and fixing r_v) such constant asymptotic values are reached at lower baryon density. Moreover, we have verified that this behavior is still realized in asymmetric hadronic matter and even in the presence of hyperons and meson degrees of freedom. This feature could be an interesting matter of investigation in future high-energy compressed nuclear matter experiments.

B. Equation of state with strange particles

Let us now investigate the EOS with the inclusion of hyperons and nonstrange and strange meson particles at fixed values of Z/A and zero net strangeness, as described in Sec. II.

In Fig. 9, the isotherms of the strange chemical potential μ_S (upper panel) and the electric charge chemical potential μ_C (lower panel) for different values of temperature and $Z/A = 0.4$ are shown. To point out the role of the Δ degrees of

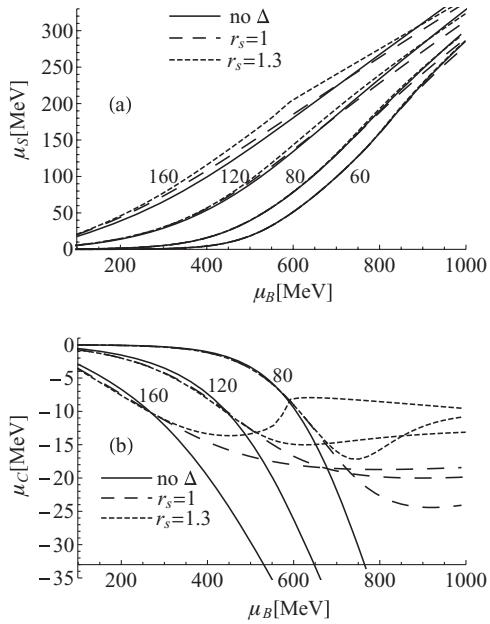

FIG. 9. Variations of the strangeness chemical potential μ_S (upper panel) and electric charge chemical potential μ_C (lower panel) with respect to the baryon chemical μ_B at different values of temperature (in MeV) and different Δ coupling constants. The parameter set is GM3 and $r_v = 1$.

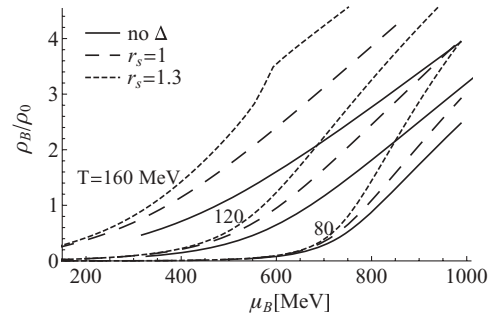

FIG. 10. Baryon density (in units of the nuclear saturation density ρ_0) as a function of the baryon chemical potential μ_B at different values of temperature (in MeV). The parameter set is GM3 and $r_v = 1$.

freedom, three different cases are considered: (i) the solid lines do not contain Δ contribution, (ii) in the long-dashed lines the Δ couplings are $r_s = r_v = 1$, and (iii) $r_s = 1.3$ and $r_v = 1$ for the short-dashed lines. As expected, for a multicomposed strange hadronic matter, μ_S is positive and increases with T and μ_B. At low T we observe very small variations in the strangeness chemical potential with different Δ coupling constants. Very significant effects instead are present in the behavior of μ_C, where, in the presence of the Δ degrees of freedom, there is a sensible reduction of its absolute value and it remains almost constant at high μ_B. This matter of fact suppresses the possibility of pion condensation also at very high baryon density (see later in this section for a further discussion on Bose condensation).

Analogously, in Figs. 10 and 11, we report, for different temperatures and $Z/A = 0.4$, the baryon density and the pressure as a function of the baryon chemical potential. One can see how the presence of the Δ degrees of freedom becomes, already for $T \approx 80$ MeV, very remarkable for baryon densities greater than about $\rho_0/2$. The parameter set used in the aforementioned calculations is GM3; however, very similar behaviors can be obtained with the other sets. As already remarked, the most relevant difference is that the presence of Δ particles occurs at lower baryon chemical potentials (baryon densities) for the TM1 EOS.

To better understand the relevance of the Δ isobars, together with the effects of the electric charge fraction and of the effective meson chemical potentials, in Fig. 12 the relative difference of the pressure $\Delta P/P$ (without and with Δs

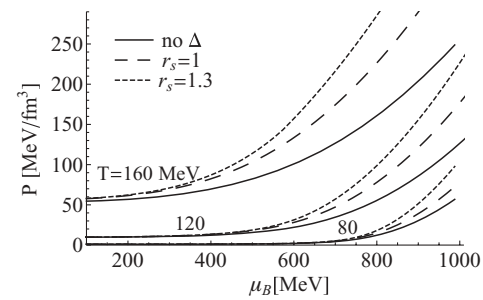

FIG. 11. Pressure as a function of the baryon chemical potential μ_B at different values of temperature (in MeV). The parameter set is GM3 and $r_v = 1$.

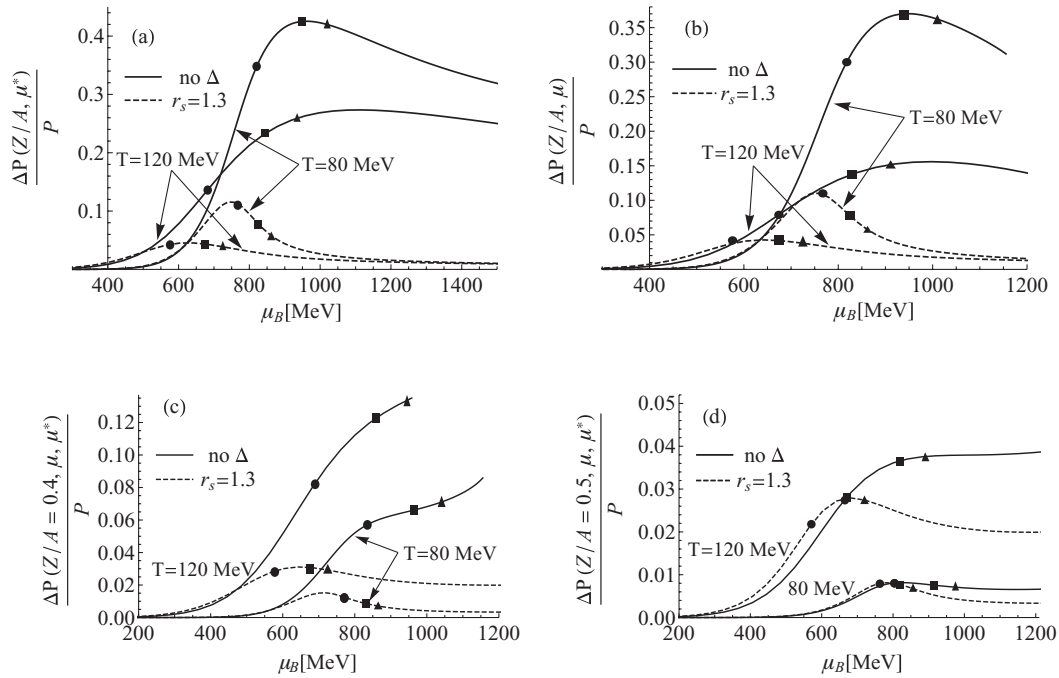

FIG. 12. Relative difference of the pressure as a function of the baryon chemical potential μ_B at different values of temperature with the exclusion (no Δ) and the inclusion ($r_s = 1.3$ and $r_v = 1$) of the Δ-isobar degrees of freedom. (a) $\Delta P(Z/A, \mu^*) \equiv P(Z/A = 0.5) - P(Z/A = 0.4)$ and the symbol μ^* means that an effective chemical potential for all hadrons has been considered (see text for details); (b) the same as panel (a) but mesons have a bare chemical potential (free boson gas); (c) $\Delta P(Z/A = 0.4, \mu, \mu^*) \equiv P(\mu) - P(\mu^*)$ at fixed $Z/A = 0.4$, where the pressure $P(\mu)$ is calculated by considering a bare chemical potential for mesons and the pressure $P(\mu^*)$ is calculated by using an effective chemical potential for all hadrons; (d) same as panel (c) but at fixed $Z/A = 0.5$. The circles, the squares, and the triangles represent the values of the baryon chemical potential corresponding to $\rho_B = \rho_0$, 2 ρ_0, and 3 ρ_0, respectively.

contribution) as a function of the baryon chemical potential is reported. The used parameter set is NL$\rho\delta$ but we have common behaviors for all three sets. In Figs. 12(a) and 12(b) the sensibility of the EOS with respect to a variation of Z/A is shown. In fact in Fig. 12(a) $\Delta P(Z/A, \mu^*) \equiv P(Z/A = 0.5) - P(Z/A = 0.4)$ and the symbol μ^* means that the effective meson chemical potentials have been taken into account, as described in Sec. II. In Fig. 12(b) the same relative difference is reported but with bare meson chemical potentials μ (in other words, all mesons are considered as a free gas of non-interacting particles). In the figure, the circles, the squares, and the triangles represent the values of the baryon chemical potential corresponding to $\rho_B = \rho_0$, 2 ρ_0, and 3 ρ_0, respectively. As expected, the EOS is more sensible to a variation of Z/A at low temperature and this effect decreases by increasing the temperature. However, this behavior is strongly related to the Δ-isobar degrees of freedom. The presence of Δ isobars greatly reduces the dependence on Z/A in the range of baryon density and temperature relevant in this investigation. This matter of fact is also realized by considering bare meson chemical potentials [Fig. 12(b)], even if this effect is less marked. As a consequence, we expect that Δ-isobar degrees of freedom affect significantly the value of the symmetric energy at finite density and temperature.

In Figs. 12(c) and 12(d), we wish to emphasize the importance of effective meson chemical potentials by considering the relative difference between the pressure $P(\mu)$, calculated with bare meson chemical potentials, and the pressure $P(\mu^*)$, including effective meson chemical potentials at fixed ratio $Z/A = 0.4$ [Fig. 12(c)] and $Z/A = 0.5$ [Fig. 12(d)]. The presence of effective meson chemical potentials reflects the behavior of the self-consistent values of the meson fields and, in particular, we see that its relevance (i) depends on the baryon density (or μ_B), (ii) increases with the temperature, (iii) depends on the isospin asymmetry (more relevant for asymmetric hadronic matter), and (iv) decreases with the presence of Δ and that the relative difference has a maximum in the region of $\rho_B \approx 0.5$–3 ρ_0. We will see in the next subsection that these features are very important in the behavior of the considered particle-antiparticle ratios and in the strangeness production.

Always concerning the role of the effective meson chemical potential, let us further observe that its absolute value is significantly lower than its bare value and, therefore, the window of μ_B and T values, in which Bose condensation can occur, appears to be greatly reduced. Considering, for example, the K^+ meson, its bare chemical potential [see Eq. (18)] is $\mu_{K^+} = \mu_S + \mu_C \equiv \mu_p - \mu_\Lambda$, which is dominated by the behavior of μ_S (that increases with μ_B and T, see Fig. 9). However, taking into account Eq. (28), $\mu^*_{K^+}$ is significantly reduced compared to μ_{K^+} by the presence of the ω- and ρ-meson fields. At fixed ratio $Z/A = 0.4$ and zero net strangeness, by increasing μ_B and T, the term containing the ρ-meson field is always negative but is much smaller than

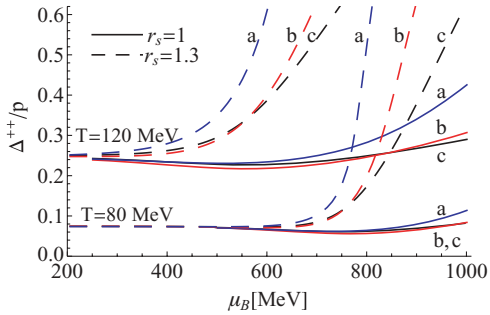

FIG. 13. (Color online) Ratios of net densities Δ^{++}/p as a function of the baryon chemical potential for different temperatures, r_s, and parameter sets (a, TM1; b, NL$\rho\delta$; c, GM3).

the (positive) ω-meson field one and, thus, kaon condensation can occur only at very high baryon densities.[2]

C. Particle ratios

This subsection starts by considering, in Fig. 13, the ratio of the net densities Δ^{++}/p as a function of the baryon chemical potential for different values of temperature and different parameters sets. As before, we fix $Z/A = 0.4$. Note that the ratio increases with the temperature but is almost constant with μ_B for $r_s = 1$. In contrast, it increases rapidly with μ_B if the Δ coupling r_s is increased. In agreement with the previous results of Figs. 6 and 8, the formation of Δ particles appears to be strongly favored for the TM1 parameter set with respect to the other two, especially for $r_s = 1.3$. Remember that, in this last case, Δ particles are in different regimes depending on the considered parameter sets (see Table IV). The aforementioned behavior should be especially evident at low-transverse-momentum pion spectra in heavy-ion collisions at intermediate/high baryon densities and temperatures. Furthermore, remembering that we are not considering decays and rescattering effects, we observe that the order of magnitude of the ratio at high temperature and low density seems to be compatible with the SPS/RHIC experimental results (with measured ratios approximately equal to 0.2–0.5) [41,42].

Figure 14 shows the variation of K^+/π^+ and K^-/π^- ratios with respect to temperature at various baryon chemical potentials, considering different parameter sets at fixed $r_s = r_v = 1$ coupling ratios. Appreciable variations between the EOSs are observed only at higher baryon chemical potentials ($\mu_B = 600$ MeV). By increasing μ_B the difference between K^+/π^+ and K^-/π^- ratios increases with the temperature but such a difference becomes much smaller at low μ_B. This behavior is in agreement with recent relativistic heavy-ion collision data [71].

[2]It is proper to remember that in this approach we are not considering effective meson masses, neglecting, for example, the repulsive potential for kaons and the attractive potential for antikaons [69,70]. Therefore, differences could occur between the present treatment and more sophisticated formulations. Please note that, in this context, there may be substantial differences between β-equilibrated nuclear matter and hot and dense nuclear matter with zero net strangeness constraint.

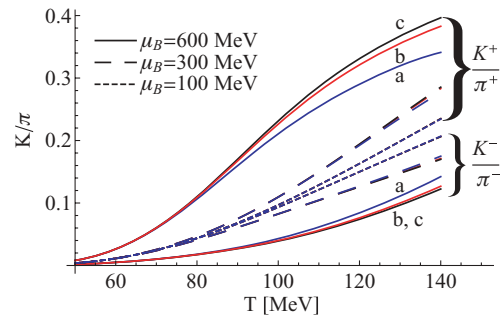

FIG. 14. (Color online) Variation of the K^+/π^+ and K^-/π^- ratios with respect to temperature at different values of baryon chemical potential and different parameter sets (a, TM1; b, NL$\rho\delta$; c, GM3). The Δ coupling ratios are fixed to $r_s = r_v = 1$.

Figure 15 shows the ratio K^+/K^- as a function of temperature at different μ_B and Δ coupling ratios (solid lines, absence of Δ's; long dashed lines, $r_s = r_v = 1$; short dashed lines, $r_s = 1.3$, $r_v = 1$); $Z/A = 0.4$. As expected, we have a value of the ratio nearly equal to one at low baryon chemical potentials ($\mu_B \leqslant 300$ MeV), while, for higher μ_B, the ratio has a peak corresponding to baryon density $\rho_B \approx 0.1$–$0.2\rho_0$ for $\mu_B \approx 500$–600 MeV curves. This nonmonotonic behavior is much more evident taking into account the Δ-isobar degrees of freedom.

To investigate how the previous results depend on the choice of the EOS, in Fig. 16, we report the variation of the K^+/K^- ratio with respect to baryon chemical potential, at fixed temperature $T = 100$ MeV and for the parameter sets GM3 and TM1 (the results relative to the NL$\rho\delta$ set are not reported because they are very close to the GM3 ones). As in Fig. 6, the higher value of r_s is fixed to the average value r_m between $r_s^{\rm II}$ and $r_s^{\rm max}$ listed in Table IV ($r_m = 1.46$ for the GM3 parameter set and $r_m = 1.30$ for TM1 parameter set). The two EOSs have similar shapes even if the ratio is suppressed at higher μ_B in the TM1 model, also in absence of Δ degrees of freedom. Moreover, a very peculiar behavior appears at $r_s = r_m$ where the ratio has a peak around $\mu_B \approx 640$–650 MeV (corresponding to $\rho_B \approx 0.7\ \rho_0$ and $\rho_B \approx \rho_0$ for TM1 and GM3 sets, respectively). This feature is mainly due to the fact that, at fixed Z/A and zero net strangeness, the density of K^+ mesons is reduced by the presence of Δ particles.

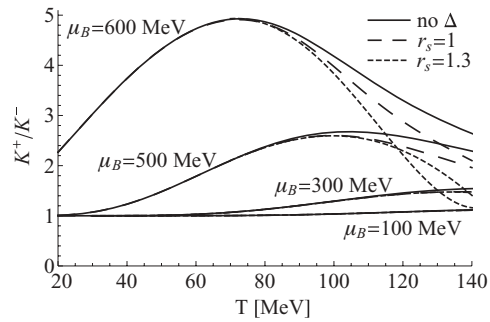

FIG. 15. Variation of the K^+/K^- ratio with respect to temperature at different values of baryon chemical potential and for different Δ coupling ratios (TM1 parameter set).

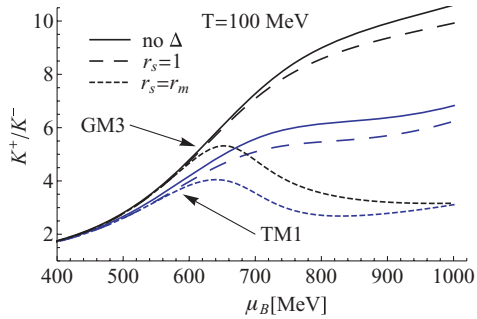

FIG. 16. (Color online) Variation of the K^+/K^- ratio with respect to baryon chemical potential at fixed temperature $T = 100$ MeV. The value r_m corresponds to the average value between $r_s^{\rm II}$ and $r_s^{\rm max}$ listed in Table IV for the two different parameter sets.

Related to the aforementioned results, it should be interesting to investigate from the experimental point of view the behavior of the ratio K^+/K^- in a kinematical region corresponding to intermediate/high temperatures and high values of μ_B.

To gain a deeper insight about the role of the Δ isobars and the net electric charge fraction, we report in Figs. 17 and 18 the variation of K^+/π^+ and K^+/K^- ratios with respect to baryon density at $T = 80$ and 120 MeV. For each temperature, we have set $Z/A = 0.4$ for solid curves and $Z/A = 0.5$ for long-dashed curves, both in the absence of Δ particles; $Z/A = 0.4$ and Δ couplings $r_s = 1.2$ for short-dashed curves; $Z/A = 0.5$ and $r_s = 1.2$ for dotted curves ($r_v = 1$). The parameter set is TM1 but similar behaviors are observed for the other two parameter sets.

Concerning the dependence on Z/A, we have to compare solid with long-dashed curves (in absence of Δ particles) and short-dashed curves with dotted ones (with the inclusion of Δ's). We can see that the differences between K^+/π^+ ratios are comparable for the two temperatures, while we have a decreasing difference between K^+/K^- ratios by increasing the temperature (it occurs as an enhancement of K^+/K^- ratios at $Z/A = 0.5$ with respect to the value $Z/A = 0.4$; the other way round takes place for K^+/π^+ ratios). As already observed in Fig. 12, the presence of the Δ isobars strongly suppresses the dependence on Z/A for the considered particle

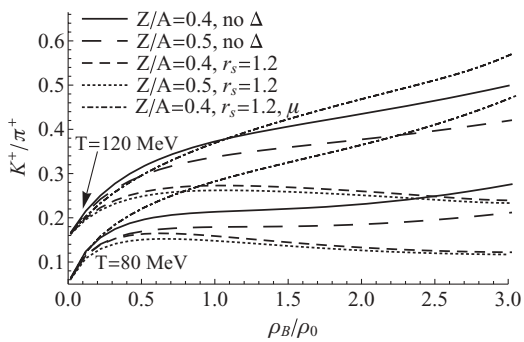

FIG. 17. Variation of K^+/π^+ ratios with respect to baryon density at $T = 80$ MeV (lower curves) and $T = 120$ MeV (upper curves). For the dash-dotted curves the symbol μ indicates that all mesons have bare chemical potentials (see text for details).

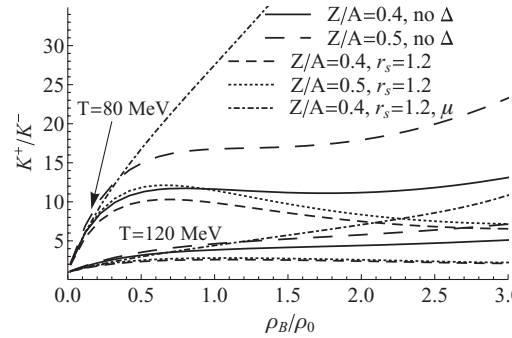

FIG. 18. The same as Fig. 17 but for K^+/K^- ratios.

ratios. However, concerning the strangeness production in the presence of the Δ-isobar degrees of freedom, we can compare solid with short-dashed curves (at fixed $Z/A = 0.4$) and long-dashed curves with the dotted ones (at fixed $Z/A = 0.5$). In agreement with the results of Figs. 14, 15, and 16, we observe that, at fixed T and ρ_B, the presence of the Δ isobars sensibly decreases both K^+/π^+ and K^+/K^- ratios. Moreover, to outline the importance of the effective meson chemical potential μ^*, in Figs. 17 and 18, we have inserted the dash-dotted curves corresponding to ratios with $Z/A = 0.4$ and Δ coupling $r_s = 1.2$, but with bare meson chemical potentials μ. As already outlined in Fig. 12, comparing these last curves with the short dashed ones, it is possible to observe the relevance of the effective meson chemical potentials at finite density and temperature and how they thus avoid unphysical too high ratios [71].

Finally, it is interesting to extend the study of the EOS also at high temperatures and low baryon chemical potential regime. At this scope, in Fig. 19, we report the results of various particle-antiparticle ratios and K^+/π^+ ratio as a function of the $\overline{p}/p$ ratio for different values of temperature. The Δ coupling ratios are fixed to $r_s = r_v = 1$ and $Z/A = 0.4$. The ratios are reported for the GM3 parameter set, however, we have verified that very close results are obtained for the other two parameter sets. Also in this case we can observe good agreement with the results obtained in the framework of statistical-thermal models [18] and with experimental SPS and RHIC data [71].

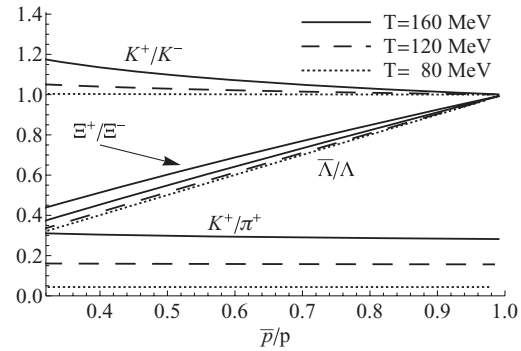

FIG. 19. Particle-antiparticle and K^+/π^+ ratios as a function of the $\overline{p}/p$ ratio for different temperatures. The Δ coupling ratios are fixed to $r_s = r_v = 1$. The ratios of Ξ^+/Ξ^- at $T = 80$ and 120 MeV are not reported because they are very strictly to the $\overline{\Lambda}/\Lambda$ ones.

IV. CONCLUSIONS

The main goal of this article is to show systematically how the presence of the Δ-isobar degrees of freedom affect the hadronic EOS by requiring, in the range of finite density and temperature, the global conservation of baryon number, electric charge fraction, and zero net strangeness. In this study we have considered three different parameter sets (GM3, NL$\rho\delta$, and TM1) that are compatible with recent analysis at intermediate-energy heavy-ion collisions and extensively adopted in several applications related to high-density β-equilibrium compact stars. We have studied a RMF model with the inclusion of the full octet of baryons and Δ-isobars, self-interacting by means of σ-, ρ-, ω-, and δ-meson fields. To take into account the lightest pseudoscalar and vector meson contributions, especially in a regime of low (but finite) baryon density and high temperature, we have incorporated the mesons as an ideal Bose gas but with effective chemical potentials. We have shown that in the EOS and, as a consequence, in the analyzed particle ratios, this assumption appears to be very relevant in the range of density and temperature considered in this article. The role of the effective meson chemical potential has a phenomenological counterpart in the excluded volume approximation for the hadron resonance gas where all effective particle chemical potentials are shifted, with respect to the real ones, proportionally to the particle excluded volume (usually assumed as a parameter). Here, from a more microscopic point of view, the effective meson chemical potentials are shifted proportionally to the meson fields, related to the self-consistent interaction between baryons.

The relevance of the Δ isobars in the EOS has been investigated for different parameter sets and coupling ratios at zero and finite temperature, in the absence and in the presence of hyperons and mesons, for symmetric and asymmetric nuclear matter. In all considered cases we have shown that the Δ-isobar degrees of freedom play a crucial role. Especially in the range of finite density and temperature considered in the last two subsections, one can see that (i) the relevance of Δ isobars strongly increases with a density and temperature increase; (ii) at fixed Z/A, the presence of Δ isobars in the EOS affects significantly the strangeness production; and (iii) Δ-isobar degrees of freedom remarkably decrease the dependence on the isospin of the EOS and, as a consequence, of the considered particle ratios. This last property appears to be very relevant also in connection to the supposed dependence on Z/A of the critical transition density from hadronic matter to a mixed phase of quarks and hadrons at high baryon and isospin density.

All quoted features are realized even if the Δ coupling ratios r_s and r_v do not necessarily correspond to the formation of a Δ-isobar metastable state; however, much stronger effects are present if we consider $r_s \gtrsim r_s^{\rm II}$ indicated in Table IV. Furthermore, apart from an appropriate variation of coupling constants, the obtained results are comparable for all three considered parameter sets. The most relevant difference is that the formation of Δ particles is favored at lower baryon density for the TM1 EOS with respect to the other two parameter sets. This matter of fact is strongly correlated to the significantly lower value of the saturated effective nuclear mass M_N^* in the TM1 parameter set.

Finally, we have investigated several particle-antiparticle ratios and strangeness production as a function of the temperature, baryon density, and antiproton to proton ratio. Although the studied EOS is principally devoted to a regime of finite and intermediate values of baryon density and temperature, a satisfactory agreement has been found with recent relativistic heavy-ion collision data and with statistical-thermal model results.

ACKNOWLEDGMENTS

It is a pleasure to thank P. Quarati for valuable suggestions and A. Drago and G. Garbarino for useful discussions.

[1] R. C. Hwa and X. N. Wang, *Quark Gluon Plasma 3* (World Scientific Publishing Co. Pvt. Ltd., Singapore, 2004).
[2] T. S. Biró, J. Phys. G: Nucl. Part. Phys. **35**, 044056 (2008); N. Armesto *et al.*, *ibid.* **35**, 054001 (2008).
[3] P. Braun-Munzinger and J. Wambach, Rev. Mod. Phys. **81**, 1031 (2009).
[4] P. Castorina, K. Redlich, and H. Satz, Eur. Phys. J. **59**, 67 (2009).
[5] P. Senger, J. Phys. G: Nucl. Part. Phys. **30**, S1087 (2004); P. Senger *et al.*, *ibid.* **36**, 064037 (2009); W. F. Henning, Nucl. Phys. A **805**, 502 (2008).
[6] I. C. Arsene *et al.*, Phys. Rev. C **75**, 034902 (2007).
[7] L. V. Bravina *et al.*, Phys. Rev. C **78**, 014907 (2008); S. Vogel, H. Petersen, K. Schmidt, E. Santini, C. Sturm, J. Aichelin, and M. Bleicher, *ibid.* **78**, 044909 (2008).
[8] S. V. Afanasiev *et al.* (NA49 Collaboration), Phys. Rev. C **66**, 054902 (2002).
[9] C. Alt *et al.* (NA49 Collaboration), Phys. Rev. C **77**, 024903 (2008).
[10] C. Höhne, Nucl. Phys. A **830**, 369c (2009).
[11] H. Caines (STAR Collaboration), arXiv:0906.0305.
[12] T. Sakaguchi (PHENIX Collaboration), arXiv:0908.3655.
[13] M. Di Toro *et al.*, Nucl. Phys. A **775**, 102 (2006).
[14] L. Bonanno, A. Drago, and A. Lavagno, Phys. Rev. Lett. **99**, 242301 (2007).
[15] T. Klahn *et al.*, Phys. Rev. C **74**, 035802 (2006).
[16] A. Drago, A. Lavagno, and P. Pagliara, Phys. Rev. D **69**, 057505 (2004); **71**, 103004 (2005).
[17] P. Braun-Munzinger, J. Stachel, and C. Wetterich, Phys. Lett. B **571**, 36 (2003); A. Andronic, P. Braun-Munzinger, and J. Stachel, Nucl. Phys. A **772**, 167 (2006); A. Andronic *et al.*, *ibid.* **789**, 334 (2007); A. Andronic, P. Braun-Munzinger, and J. Stachel, Phys. Lett. B **673**, 142 (2009).
[18] F. Becattini, J. Cleymans, A. Keranen, E. Suhonen, and K. Redlich, Phys. Rev. C **64**, 024901 (2001); F. Becattini, M. Gazdzicki, A. Keranen, J. Manninen, and R. Stock, *ibid.* **69**, 024905 (2004); F. Becattini, A. Keranen, L. Ferroni, and T. Gabbriellini, *ibid.* **72**, 064904 (2005); F. Becattini, J. Phys. G: Nucl. Part. Phys. **36**, 064019 (2009).

[19] Z. D. Lu, A. Faessler, C. Fuchs, and E. E. Zabrodin, Phys. Rev. C **66**, 044905 (2002); J. Cleymans, H. Oeschler, K. Redlich, and S. Wheaton, *ibid.* **73**, 034905 (2006); M. I. Gorenstein, M. Hauer, V. P. Konchakovski, and E. L. Bratkovskaya, *ibid.* **79**, 024907 (2009).

[20] R. Hageddorn and J. Rafelski, Phys. Lett. B **97**, 136 (1980).

[21] D. H. Rischke, M. I. Gorenstein, H. Stöcker, and W. Greiner, Z. Phys. C **51**, 485 (1991).

[22] R. Venugopalam and M. Prakash, Nucl. Phys. A **546**, 718 (1992).

[23] G. D. Yen, M. I. Gorenstein, W. Greiner, and S. N. Yang, Phys. Rev. C **56**, 2210 (1997).

[24] M. Mishra and C. P. Singh, Phys. Rev. C **78**, 024910 (2008).

[25] L. M. Satarov, M. N. Dmitriev, and I. N. Mishustin, Phys. At. Nucl. **72**, 1390 (2009).

[26] P. Danielewicz, R. Lacey, and W. G. Lynch, Science **298**, 1592 (2002).

[27] Z. Berezhiani *et al.*, Astrophys. J. **586**, 1250 (2003).

[28] B. D. Serot and J. D. Walecka, Adv. Nucl. Phys. **16**, 1 (1986).

[29] N. K. Glendenning, Phys. Rev. D **46**, 1274 (1992).

[30] J. Theis, G. Graebner, G. Buchwald, J. Maruhn, W. Greiner, H. Stocker, and J. Polonyi, Phys. Rev. D **28**, 2286 (1983); A. Delfino, M. Jansen, and V. S. Timoteo, Phys. Rev. C **78**, 034909 (2008).

[31] M. Chiapparini *et al.*, Nucl. Phys. A **826**, 178 (2009).

[32] A. Drago, A. Lavagno, and I. Parenti, Astrophys. J. **659**, 1519 (2007); W. M. Alberico and A. Lavagno, Eur. Phys. J. A **40**, 313 (2009); A. Lavagno and P. Quarati, Phys. Lett. B **498**, 47 (2001).

[33] A. S. Khvorostukhin, V. D. Toneev, and D. N. Voskresensky, Nucl. Phys. A **791**, 180 (2007); **813**, 313 (2008).

[34] D. Zschiesche *et al.*, Phys. Lett. B **547**, 7 (2002).

[35] D. Zschiesche, P. Papazoglou, S. Schramm, J. Schaffner-Bielich, H. Stocker, and W. Greiner, Phys. Rev. C **63**, 025211 (2001); D. Zschiesche *et al.*, J. Phys. G: Nucl. Part. Phys. **31**, 935 (2005); S. Vogel and M. Bleicher, Phys. Rev. C **78**, 064910 (2008).

[36] E. Zabrodin *et al.*, J. Phys. G **36**, 064065 (2009).

[37] M. Hofmann, R. Mattiello, H. Sorge, H. Stöcker, and W. Greiner, Phys. Rev. C **51**, 2095 (1995).

[38] S. Bass, M. Gyulassy, H. Stöcker, and W. Greiner, J. Phys. G: Nucl. Part. Phys. **25**, R1 (1999).

[39] G. Mao, L. Neise, H. Stöcker, and W. Greiner, Phys. Rev. C **59**, 1674 (1999).

[40] J. Schaffner *et al.*, Z. Phys. A **341**, 47 (1991).

[41] P. Fachini, J. Phys. G: Nucl. Part. Phys. **30**, S735 (2004); **35**, 044032 (2008).

[42] B. I. Abelev *et al.* (STAR Collaboration), Phys. Rev. C **78**, 044906 (2008).

[43] B. M. Waldhauser, J. Theis, J. A. Maruhn, H. Stöcker, and W. Greiner, Phys. Rev. C **36**, 1019 (1987).

[44] Z. Li, G. Mao, Y. Zhuo, and W. Greiner, Phys. Rev. C **56**, 1570 (1997).

[45] X. Jin, Phys. Rev. C **51**, 2260 (1995).

[46] D. S. Kosov, C. Fuchs, B. V. Martemyanov, and A. Faessler, Phys. Lett. B **421**, 37 (1998).

[47] H. Xiang and G. Hua, Phys. Rev. C **67**, 038801 (2003).

[48] Y. Chen, H. Guo, and Y. Liu, Phys. Rev. C **75**, 035806 (2007); Y. Chen, Y. Yuan, and Y. Liu, *ibid.* **79**, 055802 (2009).

[49] J. D. Walecka, Ann. Phys. **83**, 491 (1974).

[50] J. Boguta and A. R. Bodmer, Nucl. Phys. A **292**, 413 (1977).

[51] B. D. Serot and J. D. Walecka, Phys. Lett. B **87**, 172 (1979).

[52] B. Liu, V. Greco, V. Baran, M. Colonna, and M. Di Toro, Phys. Rev. C **65**, 045201 (2002).

[53] N. K. Glendenning, Phys. Lett. B **114**, 392 (1982).

[54] A. R. Bodmer, Nucl. Phys. A **526**, 703 (1991).

[55] N. K. Glendenning and S. A. Moszkowski, Phys. Rev. Lett. **67**, 2414 (1991).

[56] G. A. Lalazissis, J. Konig, and P. Ring, Phys. Rev. C **55**, 540 (1997).

[57] Y. Suguhara and H. Toki, Nucl. Phys. A **579**, 557 (1994).

[58] R. J. Furnstahl, J. J. Rusnak, and B. D. Serot, Nucl. Phys. A **632**, 607 (1998).

[59] J. Schaffner, C. B. Dover, A. Gal, C. Greiner, and H. Stöcker, Phys. Rev. Lett. **71**, 1328 (1993).

[60] J. Schaffner, C. B. Dover, A. Gal, D. J. Milliner, C. Greiner, and H. Stöcker, Ann. Phys. (NY) **235**, 35 (1994).

[61] R. Knorren, M. Prakash, and P. J. Ellis, Phys. Rev. C **52**, 3470 (1995).

[62] J. Schaffner and I. N. Mishustin, Phys. Rev. C **53**, 1416 (1996).

[63] J. K. Bunta and S. Gmuca, Phys. Rev. C **70**, 054309 (2004).

[64] D. J. Millener, C. B. Dover, and A. Gal, Phys. Rev. C **38**, 2700 (1988).

[65] J. Schaffner-Bielich and A. Gal, Phys. Rev. C **62**, 034311 (2000).

[66] F. Yang and H. Shen, Phys. Rev. C **77**, 025801 (2008).

[67] H. Müller, Nucl. Phys. A **618**, 349 (1997).

[68] H. Müller and B. D. Serot, Phys. Rev. C **52**, 2072 (1995).

[69] G. E. Brown and M. Rho, Nucl. Phys. A **596**, 503 (1996); G. Q. Li, C.-H. Lee, and G. E. Brown, Phys. Rev. Lett. **79**, 5214 (1997).

[70] A. Mishra, S. Schramm, and W. Greiner, Phys. Rev. C **78**, 024901 (2008); S. Banik, W. Greiner, and D. Bandyopadhyay, *ibid.* **78**, 065804 (2008).

[71] B. I. Abelev *et al.* (STAR Collaboration), Phys. Rev. C **79**, 034909 (2009), and references therein.